

Fabricating Oxidized Cellulose Sponge for Hemorrhage Control and Wound Healing

Shengyu Li,^{*,#} Xijin Wu,[#] Ningning Bai, Jianyu Ni, Xianli Liu, Weiye Mao, Lu Jin, Hai Xiang, Huiying Fu,^{*} and Qiyang Shou^{*}

Cite This: <https://doi.org/10.1021/acsbmaterials.3c00018>

Read Online

ACCESS |

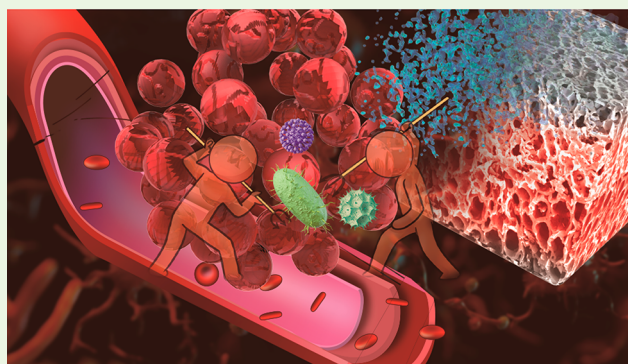
Metrics & More

Article Recommendations

Supporting Information

ABSTRACT: Uncontrolled hemorrhage and infection are the main reasons for many trauma-related deaths in both clinic and battlefield. However, most hemostatic materials have various defects and side effects, such as low hemostatic efficiency, poor biocompatibility, weak degradation ability, and lack of antimicrobial properties. Herein, an oxidized cellulose (OC) sponge with antibacterial properties and biosafety was fabricated for hemorrhage control and wound healing. The as-prepared OC sponges were prone to water triggered expansion and superabsorbent capacity, which could facilitate blood component concentration effectively. Importantly, they had significant biodegradability with little irritation to the skin. This hemostat could also reduce the plasma clotting time to 53.54% *in vitro* and demonstrated less blood loss than commercially available hemostatic agents (GS) in a mouse model of bleeding from liver defects. Furthermore, the biocompatibility antimicrobial properties and possible hemostatic mechanism of the OC sponge were also systematically evaluated. Importantly, the potential wound healing applications have also been demonstrated. Therefore, the materials have broad clinical application prospects.

KEYWORDS: hemostatic sponge, biodegradation, antibacterial, wound healing, biocompatibility



1. INTRODUCTION

Uncontrollable hemorrhage is the main reason for many trauma-related deaths, which is usually found in a battlefield or emergency and operating rooms.¹ It has been reported that 50% of deaths in the army are due to improper or inadequate treatment.² Unfortunately, traditional methods of hemostasis, such as suture and compression with gauze, are suitable for minor injuries and cannot be used to treat major bleeding, especially for cardiovascular, hepatic, gastrointestinal, and orthopedic treatments.^{3,4} They may lead to hemorrhagic shock or death once performed undeservedly.^{5,6} Nowadays, a wide variety of biological sources and polysaccharide-based materials have been investigated as topical hemostatic agents, such as chitosan, cellulose, gelatin, and so on (Surgicel, Celox, HemConBandage).^{7–12} Besides, polyethylene glycol and catechol monomers with antibacterial and adhesive properties are also effective hemostatic materials (Wound stat, Combat Gauze).^{13–16} In addition, some inorganic materials, such as silica or silica–aluminate and mineral zeolite are also used as hemostatic materials due to unique structure (Coseal).^{17–19} However, the applications of hemostatic agents are limited by biological safety, hemostatic effect, and high cost. For example, synthetic derived materials mainly have potential problems such as cytotoxicity and nonbiodegradability;^{20,21} biologically

derived hemostatic agents are expensive, have a short shelf life and a potential risk of viral contamination;²² and inorganic materials often cause thermal damage and inflammation in clinical application.^{23,24} Additionally, another key challenge that has been overlooked is the vulnerability of wounds to infection during hemostasis. Wound infection and frequent injuries will notably prolong wound healing, which may lead to many sequelae, especially for abscess formation.^{25,26} Therefore, it was imminently needed to develop novel applicable hemostatic and antibacterial materials for effective and express control of bleeding in a short time.

In reality, ideal hemostatic materials used *in vivo* should have rapid hemostasis, be nontoxic, and biodegradable, and have excellent antibacterial properties as well as good influence on healing of a wound without adverse or more drastic effects. Carboxymethyl cellulose (CMC) is one of the main derivatives of cellulose with high water retention, biocompatibility, and

Received: January 6, 2023

Accepted: April 18, 2023

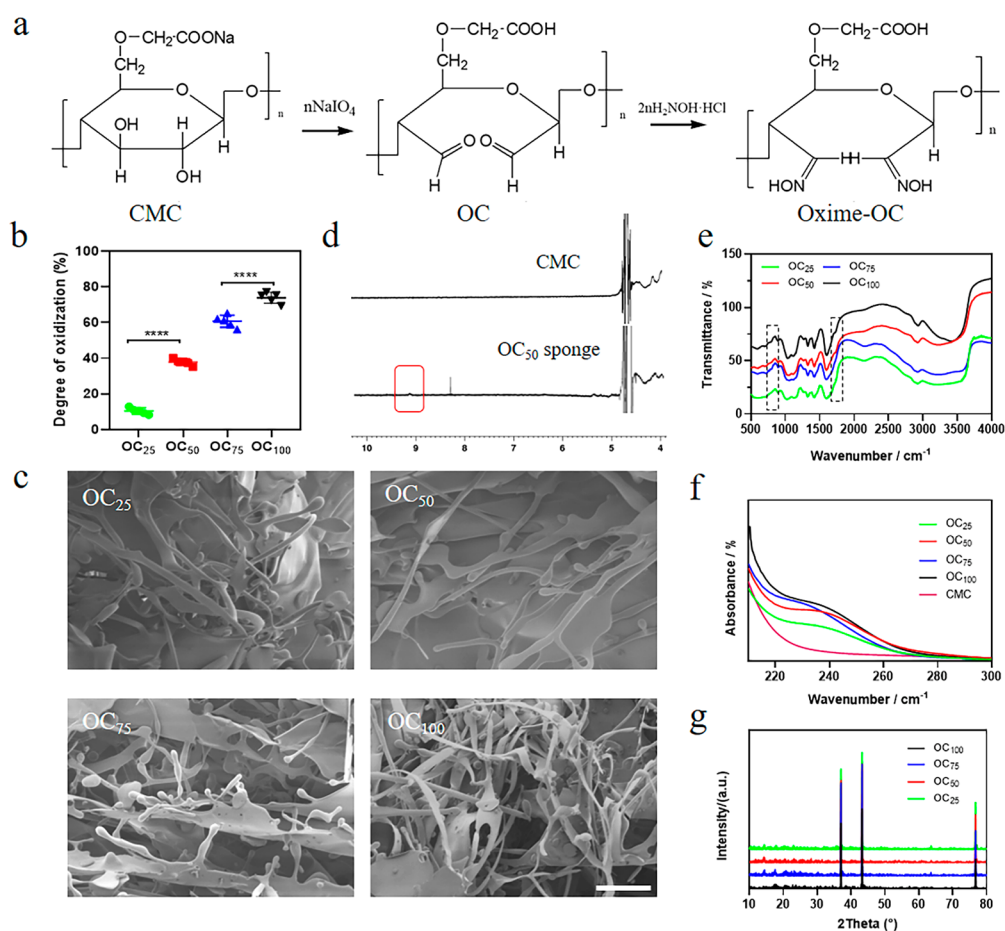


Figure 1. Synthesis and characterization of OC hemostatic sponge. (a) The illustration of periodate oxidation of CMC to OC, and conversion of OC to oxime by Schiff base reaction with hydroxylamine hydrochloride. (b) The oxidation grade of products. (c) The SEM images of materials: OC₂₅, OC₅₀, OC₇₅, and OC₁₀₀ sponges, and scale bar = 50 μm . (d) The ^1H NMR spectrum of CMC and the as-prepared OC₅₀ sponge. (e) FTIR spectra of OC sponges. (f) UV-vis and (g) XRD spectra of series of OC sponges.

biodegradability. The rich hydroxyl group confers superior modification capabilities to CMC.²⁷ In the past decade, hemostatic agents obtained by chemical modification or physical assembly of cellulose have been extensively studied. Various forms of cellulose-based hemostatic materials such as sponges, electrospun material, films, powders, and hydrogels were eventually developed (Table S1). However, most of these new hemostatic agents are designed in the form of hydrogel, and their application in the prevention and treatment of major bleeding is greatly limited, because of weak absorption performance.^{28–30} Typically, a composite hydrogel fabricated by mixing pectin and cellulose exhibited weak hemostatic and adhesive properties *in vivo* (within 3 min) as well as cellulose/keratin-catechin nanocomposite hydrogel.^{31,32} Besides, oxidized cellulose gauze (AOC) has been widely used in the treatment and hemostatic of wounds and has shown good antibacterial effect.^{33,34} However, hemostatic agents in the form of hydrogels and gauzes were not effective at absorbing blood and blocking the wound well enough to reduce the amount of bleeding.³⁵ Thus, it is important to find a suitable form of hemostatic agent that improves its performance.

The dosage forms of hemostatic drugs were abundant, including powder, gel, solution, sponge, and so on. In this work, a series of oxide-modified multifunctional cellulose (OC) sponges were prepared by lyophilization and designed for rapid hemostasis and wound healing. The oxidation process

endows the cellulose with hemostatic activity, antimicrobial properties, and biodegradability.³⁶ In this study, OC sponges with different degrees of aldehyde were characterized by UV-vis, ^1H -NMR, FT-IR, and XRD, etc. The easily biodegradable aldehydes or acetals were obtained by oxidation; OC sponges expressed a high absorption rate. The biocompatibility, antimicrobial properties, and possible hemostatic mechanism of the OC sponge were also systematically evaluated. Importantly, this hemostat showed remarkable biodegradability with little irritation to the skin. Last but not least, the potential wound healing applications have also been demonstrated.

2. MATERIALS AND METHODS

2.1. Materials. Sodium carboxymethyl cellulose (CMC, 300–800 CP) was purchased from Aladdin (Shanghai, China). Ethylene glycol (99%) was purchased from 9-Ding Chemistry Reagent Company (Shanghai, China). Sodium periodate (NaIO_4 , 99%) was purchased from Sinopharm chemical reagent (Shanghai, China). Hydroxylammonium chloride was purchased from Sigma-Aldrich (St. Louis, MO, USA). No other treatments were required for these reagents. Celox was purchased from Qingdao MeiJin R&D Ltd. (Qingdao, China). Gauze and commercial gelatin sponge (GS, Guangzhou Kuai Kang Medical Device Co., LTD) were purchased from the local hospital. *Staphylococcus aureus* (*S. aureus*, ATCC 25923) and *Escherichia coli* (*E. coli*, ATCC 25922) were purchased from Beijing Borul Kangmu Biotechnology Co., Ltd. (Beijing, China). Hematoxylin and eosin

(H&E) staining kit and Masson's trichrome staining kit were purchased from Solarbio (Beijing, China). The water (DI) was sourced from a Milli-Q Plus Ultrapure water system.

2.2. The Preparation of OC Sponge. First, CMC was dissolved in water and stirred for 24 h in the dark conditions with different ratios of sodium periodate (such as 4:1, 2:1, 4:3, 1:1, that is, the theoretical oxidation products were 25%, 50%, 75%, 100%, and the products were abbreviated as OC₂₅, OC₅₀, OC₇₅, and OC₁₀₀, respectively). Then, 1 mL of ethylene glycol was added to remove any unreacted NaIO₄. The reaction mixture was dialyzed in distilled water with a dialysis tube (Mw 3500 kDa) for 3 days to obtain pure products. Finally, the OC sponge was obtained by lyophilization of the oxidized cellulose solution.

2.3. Determination of Aldehyde Content. The degree of oxidation of CMC was evaluated by determining the content of the aldehyde group in oxidized cellulose, and the measurement method was modified with some modifications.^{27,37} As shown in Figure 1a, the OC sponge was converted to oxime through Schiff's base reaction with hydroxylamine hydrochloride. In detail the operation was as follows: the products (OC₂₅, OC₅₀, OC₇₅, and OC₁₀₀, 20 mg) were dissolved in hydroxylamine hydrochloride (5 mL, 0.25 M) solution with pH 3; then the reaction mixture was stirred gently overnight at an ambient temperature of 25 °C. The degree of oxidation was determined by the amount of hydrochloric acid in the NaOH (0.1 M) titration reaction. Finally, the oxidation degree of OCM was determined by comparing the NaOH titer volume value (0.1 M) with the standard curve of 2,4-dihydroxybenzaldehyde dosage.

2.4. Characterization. The freeze-dried sponge samples were glued to sample stage, plated with a thin layer of gold at 15 kV voltage and 20 mA current, then examined by a field emission scanning electron microscopy (FE-SEM, SU8010, Hitachi Limited, Japan). All the investigations were carried out at 2 kV voltage. X-ray diffraction (XRD) of the as-prepared samples were measured using an X-ray diffractometer (XRD-7000, Shimadzu, Japan) with Cu-K α (λ = 0.15406 nm) under reflection mode. The measurement of the samples used the following settings: step size to be 0.02°, X-ray generated at 40 kV and 30 mA, and the scan mode to be "Continuous Scan". The irradiation spot area on the sample was uniform by the mode of a programmable slit mode with the 1.0° divergence slit and the 1.0° scatter slit. Moreover, the excess noise was removed by fitting with built-in software. Peaks at 17.7°, 20.5°, 37.1°, 43.3°, 63.8°, and 76.7° on 2 θ are considered to belong to background (Figure S2). Additionally, there was a broad peak at an angle of 19.4° of CMC, which demonstrated typical amorphous structures, and they were simply flattened and contained into a holder of 10 mm diameter and 1 mm thickness.³⁸ The qualitative modification of the CMC and OC₅₀ sponge was confirmed by ¹H-NMR (Avanc III 600 MHz Digital NMR Spectrometer, BRUKER, Germany). FT-IR spectra were taken by using a FTIR spectrometer (Thermo Fisher Nicolet iS50, Thermo Fisher Scientific Co., Ltd., USA) against a blank KBr pellet background. Ultraviolet spectrum was taken by using a UV-vis spectrophotometer (Shimadzu UV-2550, Shimadzu Instrument Co., Ltd. China).

2.5. Blood Clot Index (BCI). Some modifications have been made to the BCI calculations compared with previous reports.³⁹ Briefly, 100 μ L of citrated blood with 5 μ L of CaCl₂ (0.2 M) was slowly dropped on the surface of the samples (OC sponge, GS, and gauze) and further incubated in a thermostatic shaker under 37 °C. After 10 min, 3 mL of DI were carefully added in the dish without perturbing the clotted blood. The blood coagulation test was assessed by measuring at a wavelength of 541 nm by the microplate reader (n = 4) (Cytation1, BioTek). The absorbency of citrated blood without CaCl₂ was selected as control. The BCI of samples was evaluated as follows:

$$\text{BCI \%} = \frac{\text{OD}(\text{sample})}{\text{OD}(\text{control})} \times 100$$

2.6. Cytotoxicity Evaluation. **2.6.1. CCK-8 Assay.** Mouse fibroblasts cell line (NIH 3T3) was selected to investigate the cytotoxicity of the OC sponge. Briefly, NIH 3T3 was inoculated in 96-

well plates at 100 cells/well and incubated in 5% FBS/Dulbecco's Modified Eagle's Medium (DMEM) for 24 h. Sterilized samples of the same quality (OC₂₅, OC₅₀, OC₇₅, OC₁₀₀, gauze, GS, Celox, 0.1 mg/mL) were immersed in the medium, then the leaching solution was added into the cells, which was changed twice a week. Culture medium was used as control. After 1, 3, 7 days' incubation, the CCK-8 assay was tested (Shanghai, China). The cell viability was calculated by the following equation:

$$\text{Cell viability \%} = \frac{\text{OD sample} - \text{OD blank}}{\text{OD control} - \text{OD blank}} \times 100$$

2.6.2. AM/PI Assay. The qualitative cytotoxicity evaluation was performed using live/dead cell viability assay. Similarly, NIH 3T3 was injected into 12-well plates at 1000 cells/well, and the leaching solution was added. After 1, 3, and 7 days incubation, the media was removed and the cells were washed with PBS for three times. Then, the cells were stained with the live/dead cell staining kit (Shanghai, China) according to the manufacturer's protocol and then observed by fluorescence microscopy (ECLIPSE TI-S, Nikon, Japan).

2.7. In Vitro Antimicrobial Activity. The antibacterial activity of OC sponge was investigated against the Gram-negative bacteria *E. coli* and Gram-positive bacteria *S. aureus*. Briefly, the bacteria were diluted in 0.9% physiological saline to reach a concentration of 1×10^6 CFU/mL. About 5 mg of gauze, GS, OC sponge, Celox, and CMC were weighed and added into 100 μ L of bacterial suspension solutions for 4 h. Then, the bacteria were applied after dilution, and viable colony units of *E. coli* and *S. aureus* were photographed and counted. Furthermore, 100 μ L of stock bacteria solution (10^7 CFU/mL) was incubated with the samples for 12 h, and the OD value (600 nm) was measured (n = 5).

2.8. Blood Proteins Absorption. Blood proteins absorption assay was calculated as previously reported with some modifications.³⁹ The serum was obtained by centrifuging the rat plasma at 3500 rpm/min at 37 °C for 15 min. About 10 mg of gauze, GS, OC₅₀ sponge, Celox, and OC₁₀₀ sponge were weighed and soaked into 200 μ L of rat serum for 10 min. Subsequently, after the residual serum was removed from all samples, 200 μ L of protein extract was added to each well. Then, the protein extract was centrifuged at 1500 rpm/min for 5 min after standing for 10 min. The supernatant of each sample containing proteins was collected. Finally, the protein concentration was quantified using the commercial BCA protein assay kit (Beijing, China) ($n \geq 3$). Cell Counting Kit-8 and Live/Dead cell staining kit were purchased from Yeasen (Shanghai, China). BCA protein assay kit was purchased from Beijing Labgic Technology Co., Ltd. (Beijing, China).

2.9. In Vitro Blood Clotting Evaluation. **2.9.1. Whole Blood Clotting Kinetics.** Whole blood clotting kinetics was calculated as previously reports with some modifications.³⁴ The whole blood clotting capability of OC₁₀₀ sponge was measured by blood clotting time compared with GS, Celox, CMC, and TCP. Activated blood was initiated by mixing 1 mL of 0.1 M CaCl₂ to 10 mL of citrated blood. Then, the activated blood (200 μ L) was promptly added to the sample well (OC₁₀₀, GS, Celox and CMC, 100 mg). At every different time (3, 6, 9, 12, and 18 min) point, deionized water (3 mL) was injected into each well for 10 min to break the unbound red blood cells (RBCs) into clots. At each time point, the solutions (100 μ L, n = 3) released from lysed RBCs were read at an absorbance at 540 nm.

2.9.2. Prothrombin Time (PT) and Activated Partial Thromboplastin Time (aPTT). The coagulation tests including PT and aPTT were performed as previously reported.⁴⁰ First, blood in ACD tubes provided by SD rats was centrifuged at 3000g for 15 min to obtain platelet-poor plasma (PPP). Second, 270 μ L of normal PPP and 3 mg of samples were incubated at 37 °C. After 3 min, 30 μ L of CaCl₂ (0.2 mol/L) was pipetted, and clotting time was collected. The aPTT test was performed by mixing 50 μ L of PPP with 50 μ L of aPTT reagent (Shanghai Yaji Biotechnology Co., LTD, China). After incubation for 3 min under 37 °C, 50 μ L of CaCl₂ (25 mM) and the test specimen were added into the test tube at the same time and aPTT was recorded immediately (n = 4).

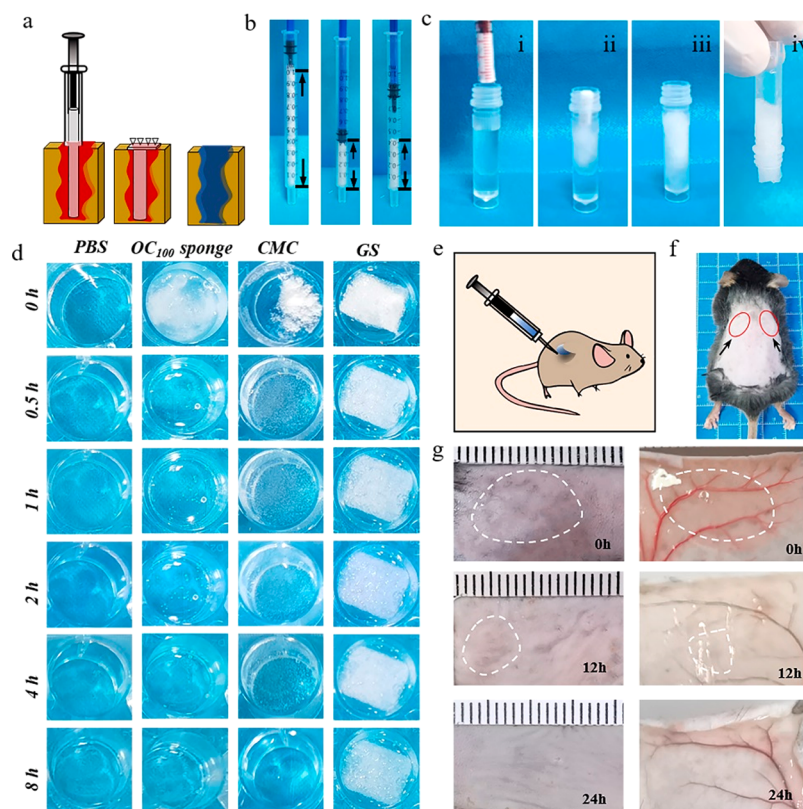


Figure 2. Swelling and shape recovery property of the OC₁₀₀ sponge. (a) Schematic drawing of the injectability and water-absorbable volume expansion for OC₁₀₀ sponges. (b) The compression properties and injectability of OC₁₀₀ sponge. (c) Water-triggered swelling properties of OC₁₀₀ sponges. (d) Digital photos of OC₁₀₀ sponge, CMC, and GS *in vitro* degradation. *In vivo* degradation of OC₁₀₀ sponge (e, simulated and f, apparent maps). (g) The photos showed the subcutaneous implants of OC₁₀₀ solution.

2.9.3. Thrombin–Antithrombin Complex (TAT). Samples (gauze, GS, Celox, and OC₁₀₀) were cocultured with 100 μ L of PPP for 10 min under 37 $^{\circ}$ C. The levels of TAT were assessed by an ELISA kit (Shanghai Yaji Biotechnology Co., LTD, China) as per the instruction of the manufacturer.

2.10. *In Vitro* and *In Vivo* Degradation Assays. To evaluate the degradation ability of OC sponges, the materials were soaked in PBS at 37 $^{\circ}$ C. In this experiment, GS and CMC were selected as controls. At a given time period, the states of all these materials were captured by the camera and the corresponding pictures were given in this paper.

In vivo degradation assays were performed using healthy male C57/BL6 mice from Zhejiang Chinese Medicine University (6–8 weeks, weight 20–22 g). About 150 μ L of 15% OC₁₀₀ sponge solution was injected into the subcutaneous area on the dorsum of mice using a syringe. Then mice were sacrificed at 0 h, 12 h, and 24 h, and the changes in subcutaneous solution were observed and recorded.

2.11. *In Vivo* Hemostatic Test. The details of a liver injury model can be found in a previous study.³⁹ The healthy male C57/BL6 mice were deeply anesthetized, and the middle lobe of liver was exposed surgically on the abdomen. Then, the left middle lobe of the liver was pierced by a disposable syringe needle (7#). The materials (gauze, GS, OC sponge, and Celox) were covered on the injury site without compression after 15 s of free bleeding, and the blank control group was left untreated. The clotting time and blood loss were recorded ($n \geq 6$).

2.12. Animal Experiments for Wound Healing. Skin wound healing experiments were carried out according to previous reports with some revisions.⁴¹ Male C57/BL6 mice (20 to 25 g) were anesthetized with 0.3% sodium pentobarbital. Two dorsal skin traumas with 1 cm long on the back were fabricated. Then, the incision area was covered by the OC hemostatic sponge immediately. A wound was sutured surgically and one was left untreated (3M) to

be used as positive control and negative control, respectively. After 7 days later, the mice were sacrificed, and the skin tissue from the incision site was taken for histological evaluation ($n = 4$).

2.13. *In Vivo* Biosafety Study. H&E staining was used to evaluate the biocompatibility of hydrogels. The sacrificed mice and the major organs (heart, liver, spleen, lung, and kidney) from each group were harvested for histological staining and observed.

The animal experiment protocol listed above had been reviewed and approved by Laboratory animal management and ethics committee of Zhejiang Chinese Medicine University (approval no. IACUC202104-0138).

2.14. Statistical Analysis. The data were expressed as the mean \pm standard deviation (SD), and the statistical analysis was performed by one-way analysis of variance (ANOVA) with GraphPad Prism 8. The values of $p < 0.05$ were considered statistically significant. The significance levels were set at * $p < 0.05$, ** $p < 0.01$, *** $p < 0.001$, and **** $p < 0.0001$.

3. RESULTS AND DISCUSSION

3.1. Characterization of OC Sponge. OC sponge was obtained through the oxidation reaction of hydroxyl (–OH) on the CMC backbone. Theoretically, 1 mol of CMC consumes 1 mol of NaIO₄ (Figure 1a). The oxidation degree of the OC sponges was measured by the hydroxylamine hydrochloride method and conducted 4 times under the same conditions to ensure the veracity. The aldehyde contents of the resulting OC were actually $8.3 \pm 1.38\%$, $37.33 \pm 1.49\%$, $61.24 \pm 4.54\%$, and $75.15 \pm 2.39\%$, and they were marked as OC₂₅ sponge, OC₅₀ sponge, OC₇₅ sponge, and OC₁₀₀ sponge, respectively (Figure 1b). The relevant yields of these samples were $36.40 \pm 4.36\%$, $34.57 \pm 3.92\%$, $34.25 \pm 3.68\%$, $88.13 \pm$

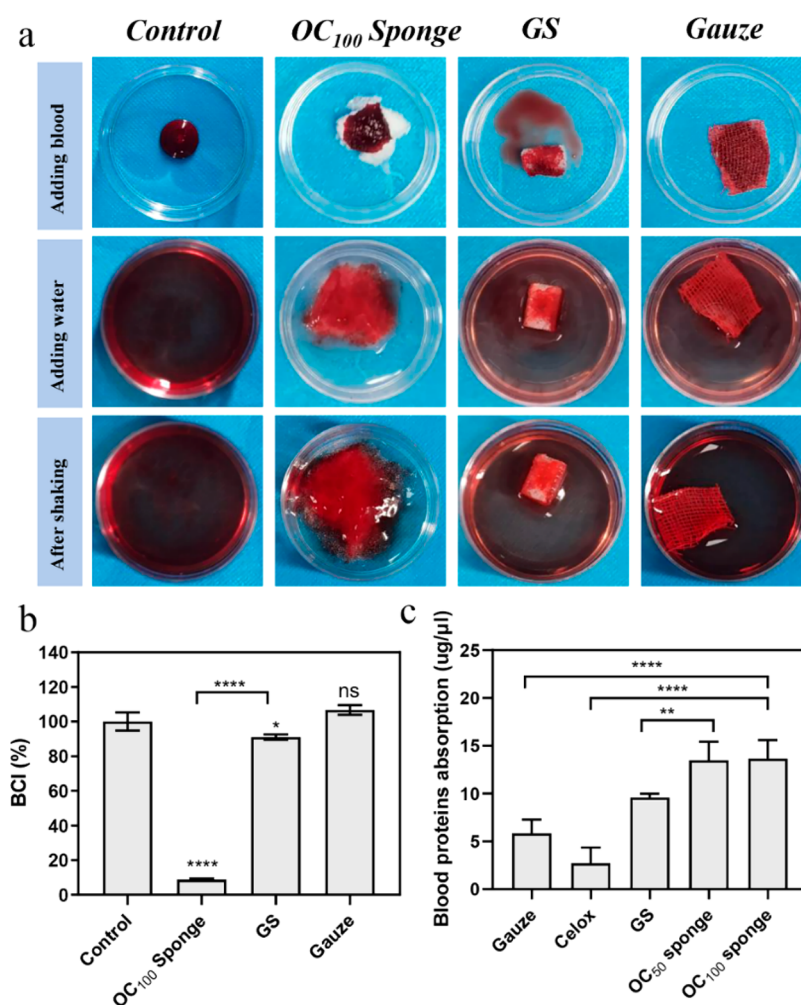


Figure 3. *In vitro* hemostatic capacity evaluation of OC₁₀₀ sponge. (a) Photographs of the blood clotting index process. (b) BCI quantitative result of OC₁₀₀ sponge; untreated served as negative control, while gauze-treated and GS served as positive control, respectively. (c) The blood protein absorption of gauze, Celox, GS, OC₅₀ sponge, and OC₁₀₀ sponge (** $p < 0.01$, **** $p < 0.0001$ and $n = 3$).

2.04%, and $36.50 \pm 2.42\%$ (w/w), respectively (Figure S1). FE-SEM micrographs of OC sponges with different aldehyde contents were shown in Figure 1c. All sponges exhibited fibrous structures. The average diameters of the OC sponges were calculated from images, using the Graph Pad Prism-8.0.1 (15–20 diameters per specimen). The size of the OC₂₅ sponge, OC₅₀ sponge, OC₇₅ sponge, and OC₁₀₀ sponge was 5.01 ± 1.55 , 5.7 ± 1.59 , 4.88 ± 1.59 , and 4.56 ± 1.32 μm , respectively (Figure S2).

The chemical structure of the OC sponges was characterized by ¹H-NMR, FT-IR, and UV-vis. First, the solvent peak of D₂O appeared at 4.8 ppm in the ¹H-NMR spectrum (as shown in Figure 1d). Also, the reference peak of starch at 9.5–10 ppm contributing to the –CHO group in the OC₅₀ sponge was clearly visible in the spectrum (the box marked red), while the hydrogen peaks of the hydroxyl group were generally not easy to appear due to their activity.⁴² Then, the FT-IR spectra of OC sponges with different aldehyde contents was shown in Figure 1e. A peak at 3472 cm^{-1} was the O–H stretching vibration of hydroxyl groups; the peak at 2916 cm^{-1} was due to the –CH₂ stretching vibration. A peak at 1416 cm^{-1} was ascribed to the C–H bending vibrations of the methylene. It should be noted that a peak at 1730 cm^{-1} was the characteristic absorption band of carbonyl groups in OC

sponges, the intensity of which was relatively weak, especially for OC₂₅ sponges.²⁹ This may be because the OC sponge formed a hemiacetal structure between the aldehyde and the unoxidized CMC during the preparation. And the vibration peak of 890 cm^{-1} was related to the hemiacetal structure (black frame).³³ As the degree of OC sponge oxidation increased, the further UV-vis spectrum exhibited an increased absorption peak at 228 nm, attributable to the aldehyde group (Figure 1f). Figure 1g and Figure S3 show the XRD pattern graphs of pure CMC and the OC sponges. Although the 2θ degree of the OCM sponges was slightly lower than that of pure CMC, all the XRD patterns were generally similar to each other and showed an amorphous structure (peaks at 17.7° , 20.5° , 37.1° , 43.3° , 63.8° and 76.7° on 2θ were considered to belong to background).

3.2. Injectability and Water-Absorbable Expansion.

The ideal hemostatic material should have the characteristics of rapid and efficient water absorption and swelling properties, which could facilitate the concentration of blood component, fill the wound effectively, compress the blood vessels, and form a physical barrier for hemostasis, especially in the compressed state. As shown in Figure 2a, OC₁₀₀ sponge could be compressed and injected into the trauma cavity. Once it triggered water, the porous sponge structure with intercon-

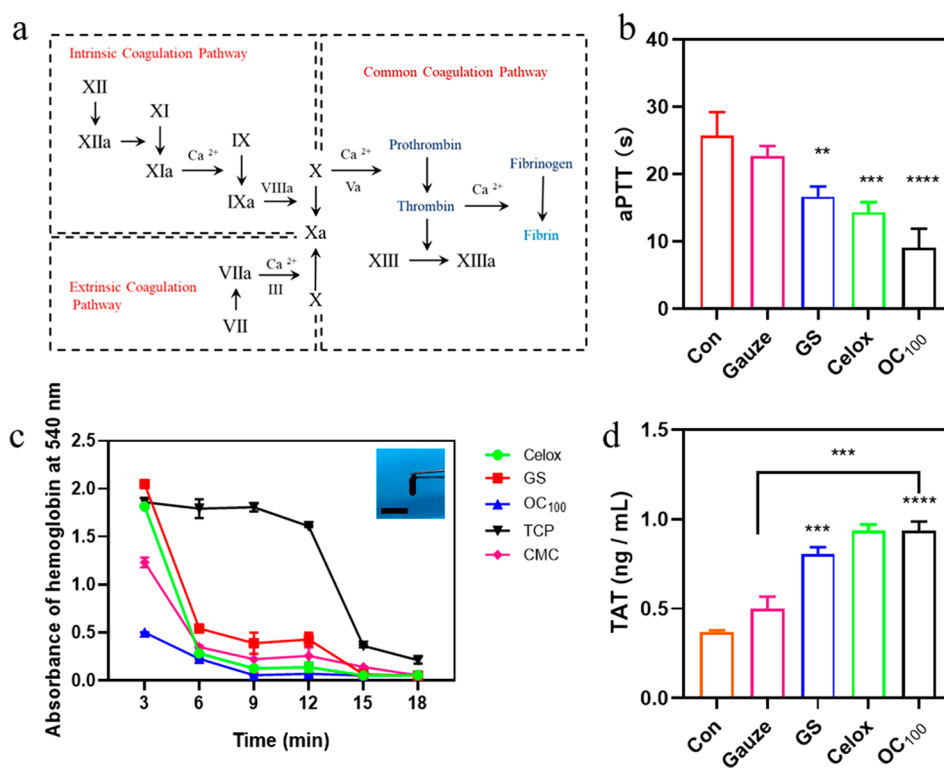


Figure 4. Coagulation factors activation of OC₁₀₀ sponges. (a) Process of the coagulation cascade, including internal and external coagulation pathways (including the common pathway). (b) aPTT measurement of gauze, GS, Celox, and OC₁₀₀ sponges ($n = 5$). (c) The whole blood clotting kinetics after adding blood on the material surfaces ($n = 3$). The insets show representative images of plasma with OC sponge for 3 min (scale bar = 0.5 cm). (d) Thrombin–antithrombin complex of thrombin generation over time. Data represent the mean \pm SD ($n = 3$), ** $P < 0.01$, *** $P < 0.001$, and **** $P < 0.0001$.

nections expanded immediately until the cavity was completely filled. As shown in Figure 2b, the OC₁₀₀ sponge turned into a half of the original volume after compression, which showed its injectability. In addition, due to the porous structure of the sponges, the compressed OC₁₀₀ sponge immediately expanded and completely fell into the container when encountering water (Figure 2c). The injectable and absorbent expansion properties of OC₁₀₀ sponges made them potentially useful for hemostasis in wounds too deep to enter bleeding areas and in irregular wounds.

3.3. In Vitro and In Vivo Degradation Study. Non-degradable biological materials might cause serious physiological reactions and even damage to organs after entering the human body. As shown in Figure 2d and Figure S4, the dissolution performance of OC sponges, CMC, and GS was observed by taking photographs within a certain time, and CMC and GS were used as positive control and negative control, respectively. Obviously, OC₁₀₀ sponges dissolved rapidly at the first half hour, while CMC degraded within 4 h slowly, which may be due to the fracture of weak hydrogen bonds and hemiacetal.³⁴ In addition, the degradability of the OC₁₀₀ sponge was further evaluated by subcutaneous implantation of mice (Figure 2e–g). These OC₁₀₀ sponge implants were also histologically stained for the intensity of the inflammatory response (Figure S5). Surprisingly, a small amount of OC₁₀₀ sponge solution remained after 12 h implantation, and all implants disappeared after 24 h (Figure 2g). According to histological section analysis in Figure S5, 15% OC₁₀₀ sponge solution hardly induced the occurrence of inflammatory reaction compared with a blank control. The above results indicated that the OC₁₀₀ sponge was a

biodegradable material, which can be rapidly degraded and absorbed *in vivo* but has a mild inflammatory reaction to tissues.

3.4. In Vitro Hemostasis Performance of OC₁₀₀ Sponge. In this work, the blood-clotting capability of OC sponges was evaluated *in vitro* by blood clot index. Figure 3a showed the digital images of the BCI process. It could be observed that the OC₁₀₀ sponge exhibited excellent blood contact efficiency, and almost no blood was diffused into DI. Additionally, the color of OC₁₀₀ sponge slightly changed after shaking, indicating blood could coagulate within 5 min automatically. As shown in Figure 3b, the BCI quantitative result of the OC₁₀₀ sponge ($7.03 \pm 2.26\%$) was significantly lower than that of GS ($82.56 \pm 6.73\%$) and gauze ($86.05 \pm 0.95\%$), expressing a better clotting ability of the OC₁₀₀ sponge. Furthermore, the blood proteins absorption of the OC sponges (OC₅₀: $5.83 \pm 1.45 \mu\text{g/mL}$; OC₁₀₀: $13.66 \pm 1.94 \mu\text{g/mL}$) was higher than that of gauze ($5.83 \pm 1.45 \mu\text{g/mL}$), Celox ($5.83 \pm 1.45 \mu\text{g/mL}$), and GS ($9.60 \pm 0.39 \mu\text{g/mL}$) (Figure 3c). Interestingly, the water absorption ($2900.85 \pm 1002.78\%$) and blood absorption ($2702.22 \pm 251.28\%$) of OC₁₀₀ sponges were also higher than that of gauze ($822.60 \pm 82\%$ and $1068.82 \pm 206.30\%$), respectively, (Figure S6 and Figure S7).

As shown in Figure 4a, the coagulation process was mainly divided into three pathways, the extrinsic, intrinsic, and common path, when the coagulation cascade was initiated. The prothrombin time (PT) and activated partial thromboplastin time (aPTT) tests are key parameters to evaluate the effects of hemostatic materials on the external and intrinsic pathways of coagulation. As shown in Figure 4b and Figure S8,

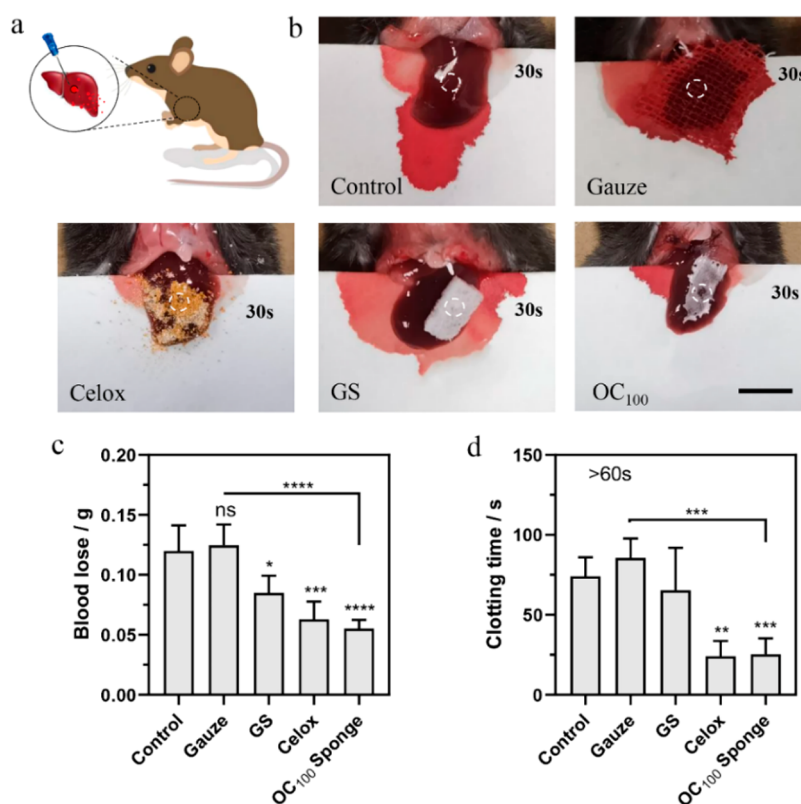


Figure 5. Hemostatic ability of OC₁₀₀ sponge. (a) Schematic diagram and (b) snapshot of the treated mouse liver hemorrhage model; untreated tissue and gauze-treated tissue were considered negative control; Celox-treated and GS-treated livers served as positive control. (d) Hemostasis time and (c) blood loss of the liver defect models. (Scale bar: 1 cm, * $p < 0.05$, ** $p < 0.01$, *** $p < 0.001$ and $n \geq 4$).

the PT and aPTT of the OC sponge-treated plasma were decreased dramatically. In addition, we further determined the impacts of the OC sponge on plasma coagulation kinetics.⁴³ In Figure 4c, the whole blood from the OC sponge showed a significantly faster coagulation rate before 6 min compared to that of control groups. All of these decreasing may be due to activating the intrinsic pathway, and then stimulating the thrombin to form a common coagulation pathway (Figure 4a).² To confirm this hypothesis, we detected the formation of the thrombin–antithrombin complex (Figure 4d). The results demonstrated that the TAT level of OC₁₀₀ sponges (0.90 ± 0.047 ng/mL) was substantially higher than that of the gauze group (0.49 ± 0.066 ng/mL) and control group (0.37 ± 0.009 ng/mL). This implicated that the incorporation of sponges does shorten the clotting time by coagulation factors activation.²⁴

3.5. In Vivo Hemostasis. The hemostatic performance of OC₁₀₀ sponge was further evaluated by measuring the amount of blood loss and hemostatic time in a mouse liver injury model (Figure 5a,b). The commercial gauze, GS, and Celox were all employed as control group. As shown in Figure 5c, OC₁₀₀ sponges presented lower blood loss significantly than that of the blank group, GS, and gauze groups, which was consistent with the results of hemostatic time (Figure 5d), and there was no significant difference between Celox and the OC₁₀₀ sponge. Moreover, the blood clotting times of Gauze and GS were about 306.75 ± 42.06 s and 306.75 ± 42.06 s, which were in line with that of whole blood without any treatment (299.2 ± 25.79 s). By comparison, the blood clotting time of the OC₁₀₀ sponge was much faster (134.5 ± 24.58 s) (Figure S9).

3.6. Cytotoxicity and Antibacterial of OC₁₀₀ Sponge.

Moreover, the cytotoxicity of OC₁₀₀ sponge on NIH 3T3 cells was evaluated by CCK-8 and live/dead staining. The commercial gauze, GS, and Celox were all employed as control group. Figure 6a showed that the cell survival rate was higher than 95% after coculture with all samples within 1 day. However, viabilities of the cells, after cocultured with Celox were only about 50% after 3 days which exhibited that Celox showed slight cytotoxicity. The same result occurred on the seventh day, which demonstrated that Celox was time-efficient. Interestingly, after a coculture with OC₁₀₀ for 7 days, the viabilities of the cells were still higher than 100%, which showed a superior cytocompatibility of OC sponges.

The proliferate of OC₁₀₀ sponge exposure on NIH 3T3 cells was investigated at different incubation times (Figure 6b). The live (green) and dead (red) cells were stained with fluorescent dyes and observed under a fluorescent microscope. It was very clearly observed the proliferation rate of OC₁₀₀ sponge-treated cells was significantly faster than that of other groups on day 3, and the cell differentiation was obvious. In addition, after 7 days of culture, OC sponges appreciated more rapidly, even if there was little difference from the control group. The above results indicated that OC sponge can not only promote cell proliferation but also has no obvious cytotoxicity and was able to be a potential hemostatic agent.

Antibacterial performance is another important index to evaluate hemostatic agents. As shown in Figure 6c, bacterial coculture results showed that OC₁₀₀ sponge had superior antibacterial properties against *E. coli* and *S. aureus*. Quantitative analysis showed that the bactericidal rate of Celox and OC₁₀₀ sponges against *S. aureus* and *E. coli* was all

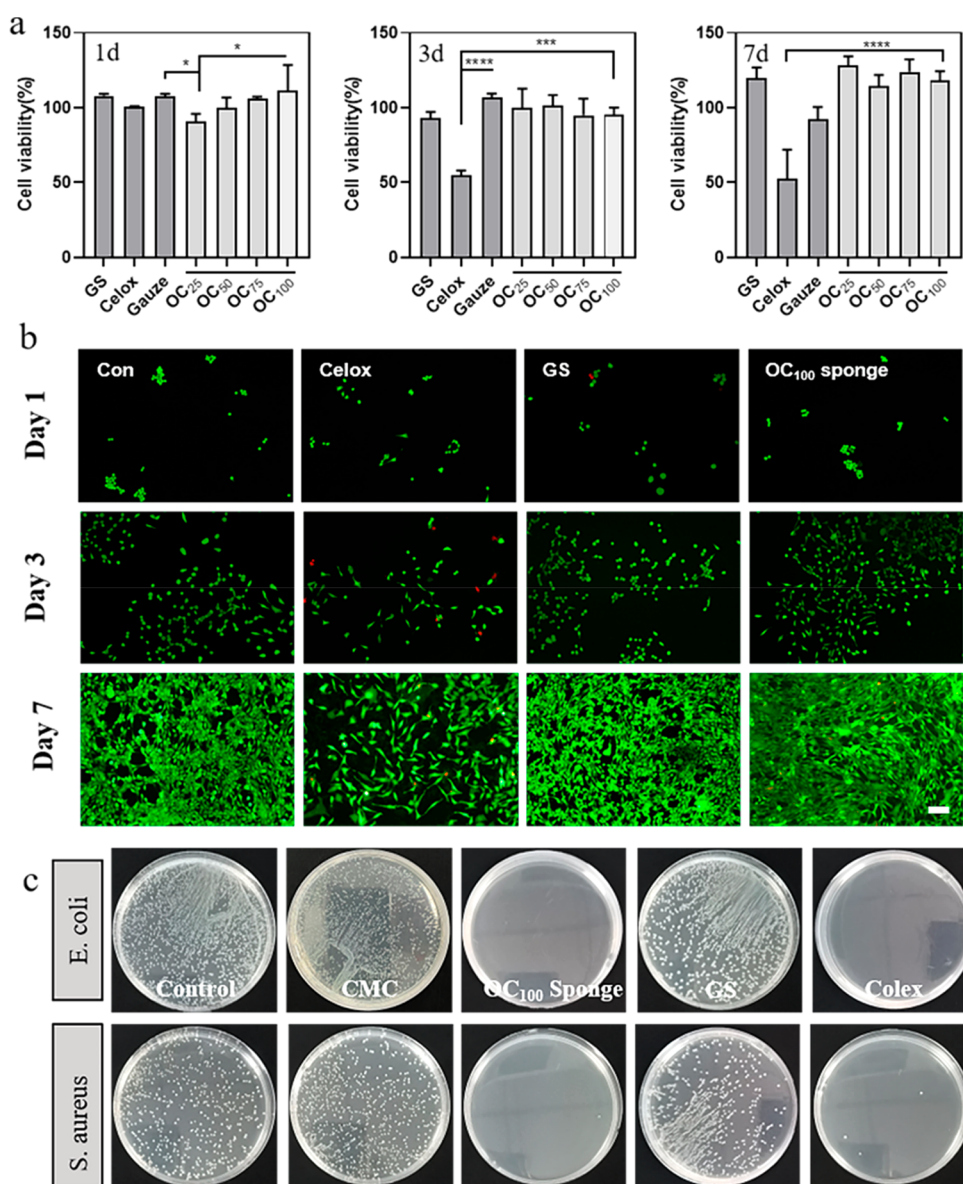


Figure 6. Cytotoxicity and antibacterial ability of OC₁₀₀ sponges. (a) Cytotoxicity of OC₁₀₀ sponge exposure on NIH 3T3 after 1, 3, and 7 days incubation. Data represent the mean \pm SD ($n = 4$). (b) Live/dead cell staining of CeloxTM, GS, OC₁₀₀ sponge exposure on NIH 3T3 cells after 1, 3, and 7 days incubation. The live (green) and dead (red) cells were stained with fluorescent dyes and observed under a fluorescent microscope. Scale bar = 100 μ m. (c) In vitro antimicrobial performance of OC₁₀₀ sponges against Gram-negative *E. coli* and Gram-positive *S. aureus*, respectively. Digital images of bacterial colonies incubated with OC₁₀₀ sponges.

above 99% (Figure S10 and Figure S11). Furthermore, the optical density (OD₆₀₀) of *E. coli* and *S. aureus* was significantly higher in gauze and GS than in Celox and OC₁₀₀ sponges (Figure S12 and Figure S13). These results confirmed that OC₁₀₀ sponge possesses great antibacterial ability.

3.7. Wound Healing. Besides being effective to hemostasis, the OC₁₀₀ sponge could also be used for effective skin wound repair due to dosage form and biodegradability. In this work, the potential application of the OC₁₀₀ sponge on wound healing was also assessed. As shown in the mouse skin incision model (Figure 7a,b), the wound incision treated with OC₁₀₀ sponge demonstrated high efficiency in wound healing after 7 days. In comparison with the OC₁₀₀ sponge and suture groups, the positive control (3M) still had scars after 7 days of treatment (Figure 7b). As shown in Figure 7c,e, the results of H&E staining confirmed that wounds treated with OC₁₀₀

sponge showed the narrowest granulation tissue gap, indicating the faster recovery of wounds. Furthermore, the more obvious collagen deposition is discovered in the wounds treated with OC sponges, indicating that they lead to a more maturely recovered skin (Figure 7d,f). In addition, OC₁₀₀ sponges facilitated wound healing and re-epithelialization, and showed a smooth appearance without further manipulation, whereas the suture-treated group required removal of sutures and repositioning by a professional. The results exhibited the remarkable advantages of OC₁₀₀ sponge, which can effectively improve wound healing.

Besides, major organs such as heart, liver, spleen, lung, and kidney were collected and stained with H&E for histological evaluation. Indeed, the H&E results of OC sponge revealed no detectable damage in comparison with that of 3M groups (Figure 7g), which validated the *in vivo* safety.

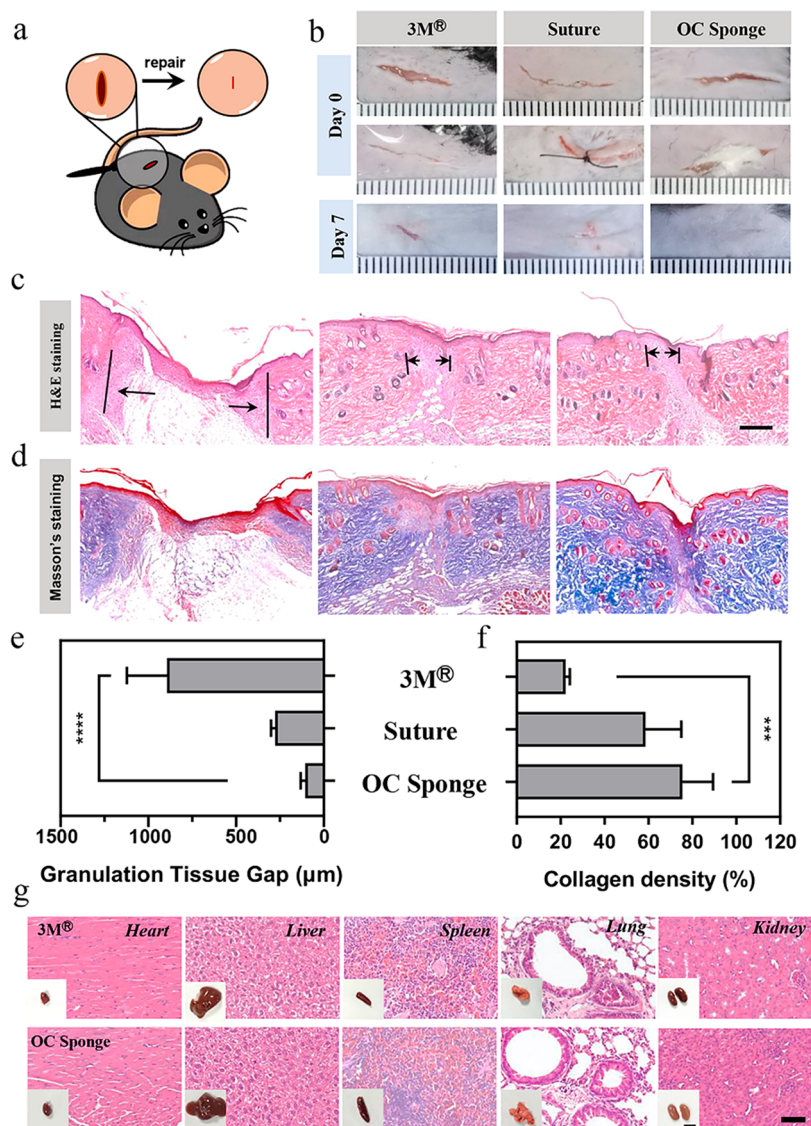


Figure 7. *In vivo* wound healing. (a) Schematic illustration of skin closure and repair assay by 3M (positive control), sutures (negative control), and OC sponge in a mice skin incision model. (b) Representative images of wounds at day 7 after different treatments. H&E (c) and Masson's trichrome staining (d) images of wound tissues on day 7 after 3M, sutures, and OC sponge treatments. The granulation tissue gaps were indicated by black arrows in H&E staining. Scale bar = 200 μm . Bar diagram of the statistic results of granulation tissue gap (e) and collagen deposition (f). *** $P < 0.001$, **** $P < 0.0001$, $n > 3$. (g) H&E staining for major organs of mice treated with 3M and OC sponge for biosafety evaluation (scale bar = 50 μm). The insets show representative images of major organs (scale bar = 1 cm).

4. CONCLUSIONS

We have successfully synthesized a series of aldehyde modified cellulose hemostatic sponges. The as-prepared OC sponge (amount of aldehyde 75.15%) with superabsorbent capacity not only showed great biodegradability *in vitro* and *in vivo*, but also displayed little skin irritation. Importantly, the hemostatic effect *in vivo* and *in vitro* of the OC sponges has been proven to be more successful than that of the commercial gelatin sponge and Celox powder. Additionally, the OC sponge, due to excellent cytocompatibility as well as antibacterial capacity, could also significantly facilitate wound healing in a full-thickness skin defect model *in vivo*. Therefore, we believe these hemostatic sponges may be excellent candidates as hemostatic and antimicrobial materials for wound healing.

■ ASSOCIATED CONTENT

Supporting Information

The Supporting Information is available free of charge at <https://pubs.acs.org/doi/10.1021/acsbomaterials.3c00018>.

Representative various forms of cellulose-based hemostatic materials; relevant yields of OC sponges; fiber's diameters of OC sponges; additional XRD details; digital photos of sponges and Celox *in vitro* degradation; H&E photos of the skin of mice 24 h after 15% OC₁₀₀ sponge solution implantation; water absorption and blood absorption of OC₁₀₀ sponge, gauze, and GS; coagulation time of normal plasma of OC sponges; clotting time of OC₁₀₀ sponge, gauze, and GS *in vitro*; the colonies number of bacterial cocultures; quantitative result of bactericidal efficacy against *E. coli* and *S. aureus*; the optical density of *E. coli* and *S. aureus* (PDF)

■ AUTHOR INFORMATION

Corresponding Authors

Shengyu Li – The Second Affiliated Hospital & Second Clinical Medical School of Zhejiang Chinese Medical University, Hangzhou 310000, P. R. China; Jinghua academy of Zhejiang Chinese Medicine University, Jinghua 321015, P. R. China; Zhejiang Provincial Key Laboratory of Sexual function of Integrated Traditional Chinese and Western Medicine, Hangzhou 310053, P. R. China; orcid.org/0000-0002-3897-1553; Email: 18768393817@163.com

Qiyang Shou – The Second Affiliated Hospital & Second Clinical Medical School of Zhejiang Chinese Medical University, Hangzhou 310000, P. R. China; Basic Medical Sciences of Zhejiang Chinese Medical University, Hangzhou 310005, P. R. China; Jinghua academy of Zhejiang Chinese Medicine University, Jinghua 321015, P. R. China; Email: sqy133@126.com

Huiying Fu – The Second Affiliated Hospital & Second Clinical Medical School of Zhejiang Chinese Medical University, Hangzhou 310000, P. R. China; Jinghua academy of Zhejiang Chinese Medicine University, Jinghua 321015, P. R. China; Zhejiang Provincial Key Laboratory of Sexual function of Integrated Traditional Chinese and Western Medicine, Hangzhou 310053, P. R. China; Email: fhy131@126.com

Authors

Xijin Wu – The Second Affiliated Hospital & Second Clinical Medical School of Zhejiang Chinese Medical University, Hangzhou 310000, P. R. China; Zhejiang Provincial Key Laboratory of Sexual function of Integrated Traditional Chinese and Western Medicine, Hangzhou 310053, P. R. China

Ningning Bai – The Second Affiliated Hospital & Second Clinical Medical School of Zhejiang Chinese Medical University, Hangzhou 310000, P. R. China; Zhejiang Provincial Key Laboratory of Sexual function of Integrated Traditional Chinese and Western Medicine, Hangzhou 310053, P. R. China

Jianyu Ni – The Second Affiliated Hospital & Second Clinical Medical School of Zhejiang Chinese Medical University, Hangzhou 310000, P. R. China; Zhejiang Provincial Key Laboratory of Sexual function of Integrated Traditional Chinese and Western Medicine, Hangzhou 310053, P. R. China

Xianli Liu – The Second Affiliated Hospital & Second Clinical Medical School of Zhejiang Chinese Medical University, Hangzhou 310000, P. R. China; Zhejiang Provincial Key Laboratory of Sexual function of Integrated Traditional Chinese and Western Medicine, Hangzhou 310053, P. R. China

Weiyi Mao – The Second Affiliated Hospital & Second Clinical Medical School of Zhejiang Chinese Medical University, Hangzhou 310000, P. R. China; Zhejiang Provincial Key Laboratory of Sexual function of Integrated Traditional Chinese and Western Medicine, Hangzhou 310053, P. R. China

Lu Jin – The Second Affiliated Hospital & Second Clinical Medical School of Zhejiang Chinese Medical University, Hangzhou 310000, P. R. China; Zhejiang Provincial Key Laboratory of Sexual function of Integrated Traditional

Chinese and Western Medicine, Hangzhou 310053, P. R. China

Hai Xiang – Zhejiang Provincial Key Laboratory of Sexual function of Integrated Traditional Chinese and Western Medicine, Hangzhou 310053, P. R. China

Complete contact information is available at:

<https://pubs.acs.org/10.1021/acsbiomaterials.3c00018>

■ Author Contributions

#S.L. and X.W. contributed equally to this work. S.L.: conceptualization, validation, formal analysis, writing-original draft, funding acquisition, writing-review and editing. X.W.: writing-original draft, validation, formal analysis. N.B.: supervision, validation. W.M. and H.X.: writing - review & editing, supervision. J.N.: data curation, validation. X.L.: formal analysis, investigation, supervision. W.M.: formal analysis. L.J., H.F., and Q.S.: writing-review and editing, funding acquisition.

■ Notes

The authors declare no competing financial interest.

■ ACKNOWLEDGMENTS

This work was supported by Medical Health Science and Technology project of Zhejiang Province (2022RC220), Research Fund of Zhejiang Chinese Medical University (2021ZY03), The Natural Science Foundation of Zhejiang Province (LQ23H280007 to L.J.), and National Natural Science Foundation of China (82274175, 81873047 to QYS. 81673645 to H.Y.F.).

■ REFERENCES

- (1) Eastridge, B. J.; Mabry, R. L.; Seguin, P.; Cantrell, J.; Tops, T.; Uribe, P.; Mallett, O.; Zubko, T.; Oetjen-Gerdes, L.; Rasmussen, T. E.; Butler, F. K.; Kotwal, R. S.; Holcomb, J. B.; Wade, C.; Champion, H.; Lawnick, M.; Moores, L.; Blackburne, L. H. Death on the battlefield (2001–2011): implications for the future of combat casualty care. *J. Trauma Acute Care Surg* **2012**, *73*, S431–437.
- (2) Feng, C.; Li, J.; Wu, G. S.; Mu, Y. Z.; Kong, M.; Jiang, C. Q.; Cheng, X. J.; Liu, Y.; Chen, X. G. Chitosan-Coated Diatom Silica as Hemostatic Agent for Hemorrhage Control. *ACS Appl. Mater. Interfaces* **2016**, *8*, 34234–34243.
- (3) Ricardo, J. W.; Lipner, S. R. Kaolin-impregnated gauze for hemostasis following nail surgery. *J. Am. Acad. Dermatol* **2021**, *85*, No. e13–e14.
- (4) Yang, X.; Liu, W.; Li, N.; Wang, M.; Liang, B.; Ullah, I.; Luis Neve, A.; Feng, Y.; Chen, H.; Shi, C. Design and development of polysaccharide hemostatic materials and their hemostatic mechanism. *Biomater Sci* **2017**, *5*, 2357–2368.
- (5) Zheng, C.; Zeng, Q.; Pimpi, S.; Wu, W.; Han, K.; Dong, K.; Lu, T. Research status and development potential of composite hemostatic materials. *J. Mater. Chem. B* **2020**, *8*, 5395–5410.
- (6) Moldovan, H.; Antoniac, I.; Gheorghita, D.; Safta, M. S.; Preda, S.; Broasca, M.; Badila, E.; Fronea, O.; Scafa-Udriste, A.; Cacoveanu, M.; Molnar, A.; Costache, V. S.; Zaharia, O. Biomaterials as Haemostatic Agents in Cardiovascular Surgery: Review of Current Situation and Future Trends. *Polymers (Basel)* **2022**, *14*, 1189.
- (7) Ponsen, A. C.; Proust, R.; Soave, S.; Mercier-Nome, F.; Garcin, I.; Combettes, L.; Lataillade, J. J.; Uzan, G. A new hemostatic agent composed of Zn(2+)-enriched Ca(2+) alginate activates vascular endothelial cells in vitro and promotes tissue repair in vivo. *Bioact Mater* **2022**, *18*, 368–382.
- (8) Oto, A.; Remer, E. M.; O'Malley, C. M.; Tkach, J. A.; Gill, I. S. MR characteristics of oxidized cellulose (Surgicel). *AJR Am. J. Roentgenol* **1999**, *172*, 1481–1484.

- (9) Du, X.; Wu, L.; Yan, H.; Jiang, Z.; Li, S.; Li, W.; Bai, Y.; Wang, H.; Cheng, Z.; Kong, D.; Wang, L.; Zhu, M. Microchannelled alkylated chitosan sponge to treat noncompressible hemorrhages and facilitate wound healing. *Nat. Commun.* **2021**, *12*, 4733.
- (10) Burkatovskaya, M.; Tegos, G. P.; Swietlik, E.; Demidova, T. N.; P. Castano, A.; Hamblin, M. R. Use of chitosan bandage to prevent fatal infections developing from highly contaminated wounds in mice. *Biomaterials* **2006**, *27*, 4157–4164.
- (11) Jimenez-Martin, J.; Las Heras, K.; Etxabide, A.; Uranga, J.; de la Caba, K.; Guerrero, P.; Igartua, M.; Santos-Vizcaino, E.; Hernandez, R. M. Green hemostatic sponge-like scaffold composed of soy protein and chitin for the treatment of epistaxis. *Mater. Today Bio* **2022**, *15*, 100273.
- (12) Cui, Y.; Huang, Z.; Lei, L.; Li, Q.; Jiang, J.; Zeng, Q.; Tang, A.; Yang, H.; Zhang, Y. Robust hemostatic bandages based on nanoclay electrospun membranes. *Nat. Commun.* **2021**, *12*, 5922.
- (13) Zhu, J.; Li, F.; Wang, X.; Yu, J.; Wu, D. Hyaluronic Acid and Polyethylene Glycol Hybrid Hydrogel Encapsulating Nanogel with Hemostasis and Sustainable Antibacterial Property for Wound Healing. *ACS Appl. Mater. Interfaces* **2018**, *10*, 13304–13316.
- (14) Malik, A.; Inayat, F.; Goraya, M. H. N.; Shahzad, E.; Zaman, M. A. Severe Acute Colonic Diverticular Bleeding: The Efficacy of Rapid Bowel Preparation With 1 L Polyethylene Glycol Ascorbate Solution and Direct Endoscopic Hemoclippping for Successful Hemostasis. *J. Investig. Med. High Impact Case Rep* **2021**, *9*, 2324709621994383.
- (15) He, H.; Sun, C.; Weng, Y.; Huang, H.; Ni, P.; Fang, Y.; Xu, R.; Wang, Z.; Liu, H. Catechol modification of non-woven chitosan gauze for enhanced hemostatic efficacy. *Carbohydr. Polym.* **2022**, *286*, 119319.
- (16) Shin, M.; Choi, J. H.; Kim, K.; Kim, S.; Lee, H. Hemostatic Needles: Controlling Hemostasis Time by a Catecholamine Oxidative Pathway. *ACS Appl. Mater. Interfaces* **2021**, *13*, 10741–10747.
- (17) Li, J.; Han, J.; Sun, Q.; Wang, Y.; Mu, Y.; Zhang, K.; Dou, X.; Kong, M.; Chen, X.; Feng, C. Biosynthetic calcium-doped biosilica with multiple hemostatic properties for hemorrhage control. *J. Mater. Chem. B* **2018**, *6*, 7834–7841.
- (18) Shen, Y. F.; Huang, J. H.; Wu, Z. E.; Wang, K. Y.; Zheng, J.; Cai, L.; Li, X. L.; Gao, H.; Jin, X. Y.; Li, J. F. Cationic superabsorbent hydrogel composed of mesoporous silica as a potential haemostatic material. *Mater. Sci. Eng. C Mater. Biol. Appl.* **2020**, *111*, 110841.
- (19) Lokhande, G.; Carrow, J. K.; Thakur, T.; Xavier, J. R.; Parani, M.; Bayless, K. J.; Gaharwar, A. K. Nanoengineered injectable hydrogels for wound healing application. *Acta Biomater* **2018**, *70*, 35–47.
- (20) Xie, X.; Li, D.; Chen, Y.; Shen, Y.; Yu, F.; Wang, W.; Yuan, Z.; Morsi, Y.; Wu, J.; Mo, X. Conjugate Electrospun 3D Gelatin Nanofiber Sponge for Rapid Hemostasis. *Adv. Health Mater.* **2021**, *10*, No. e2100918.
- (21) Han, K.; Bai, Q.; Wu, W.; Sun, N.; Cui, N.; Lu, T. Gelatin-based adhesive hydrogel with self-healing, hemostasis, and electrical conductivity. *Int. J. Biol. Macromol.* **2021**, *183*, 2142–2151.
- (22) Yu, L.; Gu, T.; Song, L.; Shi, E.; Fang, Q.; Wang, C.; Zhao, J. Fibrin sealant provides superior hemostasis for sternotomy compared with bone wax. *Ann. Thorac Surg* **2012**, *93*, 641–644.
- (23) Wright, J. K.; Kalns, J.; Wolf, E. A.; Traweek, F.; Schwarz, S.; Loeffler, C. K.; Snyder, W.; Yantis, L. D., Jr; Eggers, J. Thermal injury resulting from application of a granular mineral hemostatic agent. *J. Trauma* **2004**, *57*, 224–230.
- (24) Wang, C.; Niu, H.; Ma, X.; Hong, H.; Yuan, Y.; Liu, C. Bioinspired, Injectable, Quaternized Hydroxyethyl Cellulose Composite Hydrogel Coordinated by Mesocellular Silica Foam for Rapid, Noncompressible Hemostasis and Wound Healing. *ACS Appl. Mater. Interfaces* **2019**, *11*, 34595–34608.
- (25) Li, S.; Chen, A.; Chen, Y.; Yang, Y.; Zhang, Q.; Luo, S.; Ye, M.; Zhou, Y.; An, Y.; Huang, W.; Xuan, T.; Pan, Y.; Xuan, X.; He, H.; Wu, J. Lotus leaf inspired antiadhesive and antibacterial gauze for enhanced infected dermal wound regeneration. *Chemical Engineering Journal* **2020**, *402*, 126202.
- (26) Ma, W.; Dong, W.; Zhao, S.; Du, T.; Wang, Y.; Yao, J.; Liu, Z.; Sun, D.; Zhang, M. An injectable adhesive antibacterial hydrogel wound dressing for infected skin wounds. *Mater. Sci. Eng. C Mater. Biol. Appl.* **2022**, *134*, 112584.
- (27) Zhu, H.; Mei, X.; He, Y.; Mao, H.; Tang, W.; Liu, R.; Yang, J.; Luo, K.; Gu, Z.; Zhou, L. Fast and High Strength Soft Tissue Bioadhesives Based on a Peptide Dendrimer with Antimicrobial Properties and Hemostatic Ability. *ACS Appl. Mater. Interfaces* **2020**, *12*, 4241–4253.
- (28) Zou, C. Y.; Lei, X. X.; Hu, J. J.; Jiang, Y. L.; Li, Q. J.; Song, Y. T.; Zhang, Q. Y.; Li-Ling, J.; Xie, H. Q. Multi-crosslinking hydrogels with robust bio-adhesion and pro-coagulant activity for first-aid hemostasis and infected wound healing. *Bioact Mater.* **2022**, *16*, 388–402.
- (29) Pang, J.; Bi, S.; Kong, T.; Luo, X.; Zhou, Z.; Qiu, K.; Huang, L.; Chen, X.; Kong, M. Mechanically and functionally strengthened tissue adhesive of chitin whisker complexed chitosan/dextran derivatives based hydrogel. *Carbohydr. Polym.* **2020**, *237*, 116138.
- (30) Guan, Q. F.; Yang, H. B.; Han, Z. M.; Ling, Z. C.; Yin, C. H.; Yang, K. P.; Zhao, Y. X.; Yu, S. H. Sustainable Cellulose-Nanofiber-Based Hydrogels. *ACS Nano* **2021**, *15*, 7889–7898.
- (31) Chen, W.; Yuan, S.; Shen, J.; Chen, Y.; Xiao, Y. A Composite Hydrogel Based on Pectin/Cellulose via Chemical Cross-Linking for Hemorrhage. *Front Bioeng Biotechnol* **2021**, *8*, 627351.
- (32) Sun, Z.; Chen, X.; Ma, X.; Cui, X.; Yi, Z.; Li, X. Cellulose/keratin-catechin nanocomposite hydrogel for wound hemostasis. *J. Mater. Chem. B* **2018**, *6*, 6133–6141.
- (33) Zhang, L.; Ge, H.; Xu, M.; Cao, J.; Dai, Y. Physicochemical properties, antioxidant and antibacterial activities of dialdehyde microcrystalline cellulose. *Cellulose* **2017**, *24*, 2287–2298.
- (34) Liu, C.; Liu, X.; Liu, C.; Wang, N.; Chen, H.; Yao, W.; Sun, G.; Song, Q.; Qiao, W. A highly efficient, in situ wet-adhesive dextran derivative sponge for rapid hemostasis. *Biomaterials* **2019**, *205*, 23–37.
- (35) Scognamiglio, F.; Travan, A.; Rustighi, I.; Tarchi, P.; Palmisano, S.; Marsich, E.; Borgogna, M.; Donati, L.; de Manzini, N.; Paoletti, S. Adhesive and sealant interfaces for general surgery applications. *J. Biomed Mater. Res. B Appl. Biomater* **2016**, *104*, 626–639.
- (36) Liu, S.; Liu, X.; Ren, Y.; Wang, P.; Pu, Y.; Yang, R.; Wang, X.; Tan, X.; Ye, Z.; Maurizot, V.; Chi, B. Mussel-Inspired Dual-Crosslinking Hyaluronic Acid/epsilon-Polylysine Hydrogel with Self-Healing and Antibacterial Properties for Wound Healing. *ACS Appl. Mater. Interfaces* **2020**, *12*, 27876–27888.
- (37) Li, H.; Wu, B.; Mu, C.; Lin, W. Concomitant degradation in periodate oxidation of carboxymethyl cellulose. *Carbohydr. Polym.* **2011**, *84*, 881–886.
- (38) Liang, Y.; Hawkins, J. E.; Ries, M. E.; Hine, P. J. Dissolution of cotton by 1-ethyl-3-methylimidazolium acetate studied with time-temperature superposition for three different fibre arrangements. *Cellulose* **2021**, *28*, 715–727.
- (39) Chen, S.; Carlson, M. A.; Zhang, Y. S.; Hu, Y.; Xie, J. Fabrication of injectable and superelastic nanofiber rectangle matrices (“peanuts”) and their potential applications in hemostasis. *Biomaterials* **2018**, *179*, 46–59.
- (40) Udangawa, R. N.; Mikael, P. E.; Mancinelli, C.; Chapman, C.; Willard, C. F.; Simmons, T. J.; Linhardt, R. J. Novel Cellulose-Halloysite Hemostatic Nanocomposite Fibers with a Dramatic Reduction in Human Plasma Coagulation Time. *ACS Appl. Mater. Interfaces* **2019**, *11*, 15447–15456.
- (41) Bai, S.; Zhang, X.; Cai, P.; Huang, X.; Huang, Y.; Liu, R.; Zhang, M.; Song, J.; Chen, X.; Yang, H. A silk-based sealant with tough adhesion for instant hemostasis of bleeding tissues. *Nanoscale Horizons* **2019**, *4*, 1333–1341.
- (42) Oikawa, M.; Adachi, S.; Kusumoto, S. 2JC,H index: a nondestructive NMR method for differentiation of aldohexopyranosyl residues. *Org. Lett.* **2005**, *7*, 661–664.
- (43) Kumar, V. A.; Taylor, N. L.; Jalan, A. A.; Hwang, L. K.; Wang, B. K.; Hartgerink, J. D. A nanostructured synthetic collagen mimic for hemostasis. *Biomacromolecules* **2014**, *15*, 1484–1490.